

ContactSDF: Signed Distance Functions as Multi-Contact Models for Dexterous Manipulation

Wen Yang, Wanxin Jin

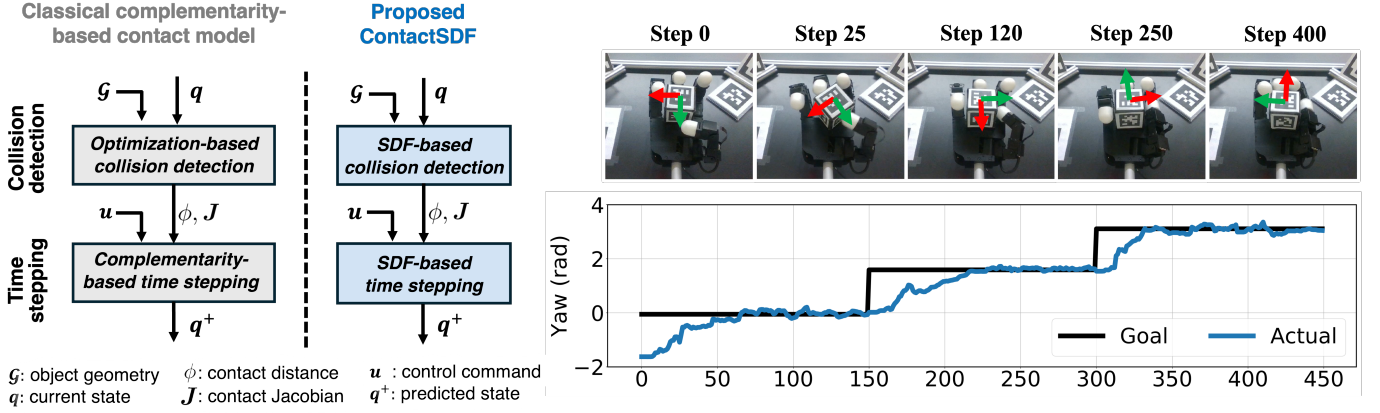


Fig. 1: Left: classic multi-contact model vs. proposed ContactSDF. ContactSDF approximates the contact detection and time-stepping routines using signed distance functions, leading to an explicit and differentiable contact model, which facilitates model-based planning and learning. Right: ContactSDF model predictive control (ContactSDF-MPC) for Allegro hand on-palm reorientation. Within 2 minutes of learning on hardware, ContactSDF-MPC enables the Allegro hand to perform continuous in-hand reorientation at control frequency of 50 Hz.

Abstract—In this paper, we propose ContactSDF, a method that uses signed distance functions (SDFs) to approximate multi-contact models, including both collision detection and time-stepping routines. ContactSDF first establishes an SDF using the supporting plane representation of an object for collision detection, and then use the generated contact dual cones to build a second SDF for time stepping prediction of the next state. Those two SDFs create a differentiable and closed-form multi-contact dynamic model for state prediction, enabling efficient model learning and optimization for contact-rich manipulation. We perform extensive simulation experiments to show the effectiveness of ContactSDF for model learning and real-time control of dexterous manipulation. We further evaluate the ContactSDF on a hardware Allegro hand for on-palm reorientation tasks. Results show with around 2 minutes of learning on hardware, the ContactSDF achieves high-quality dexterous manipulation at a frequency of 30-60Hz. [Project page](#).

I. INTRODUCTION

In dexterous manipulation, a robot must decide when and where to make and break contact with objects. The contact-rich interactions make the system dynamics hybrid and nonsmooth, creating significant challenges in model learning and control. While model-free reinforcement learning has shown impressive results in dexterous manipulation tasks, it comes at the cost of extensive data. Conversely, model-based methods, though theoretically more data-efficient, often fall short of achieving similar performance. Recent advances in contact model learning [1]–[3] and planning [4]–[6] have highlighted the importance of handling the hybrid and nonsmooth structures of contact dynamics. The complementarity-based formulations [7]–[9] are widely used in those methods. While effective in representing contact interactions, complementarity-based models are computationally non-smooth and hybrid, making them difficult to integrate into standard learning and planning

frameworks without specialized algorithm design [1], [10], [11].

To address the computational challenges of complementarity-based models, we introduce ContactSDF, a novel multi-contact model utilizing signed distance functions (SDF). ContactSDF has two key components, as illustrated in Fig. 1: (1) SDF-based collision detection, where robot and environment points query a geometric SDF that is constructed directly from the polytope representation of the object mesh or point cloud [12]; and (2) SDF-based time-stepping prediction, where a velocity-space SDF is proposed to approximate the time-stepping of multi-contact dynamics based on the contact dual cones obtained from the collision detection. With these two SDFs, the ContactSDF achieves a closed-form state dynamics and end-to-end differentiability (collision detection routine included). This makes ContactSDF easily integrated into existing model learning and optimization frameworks, allowing for efficient representation learning and real-time control in dexterous manipulation. Our contributions are summarized as follows:

- We propose ContactSDF, a multi-contact model built upon signed distance functions, which attains closed-form prediction and differentiability.
- We develop ContactSDF predictive control (ContactSDF-MPC), to achieve real-time control of dexterous manipulation. ContactSDF-MPC is then integrated into an on-MPC learning framework to further improve its performance.
- We evaluate the ContactSDF in simulation and on a hardware Allegro hand for in-hand dexterous manipulation (Fig. 1). The results show within 2 minutes of learning on hardware, ContactSDF achieves high-quality control performance for dexterous manipulation with MPC frequency of 50 Hz.

II. RELATED WORKS

A. Complementarity-Based Contact Models

The rigid body multi-contact dynamics is classically formulated as complementarity-based models [7], [9], [13], which describes non-smooth constraints on body motions and contact force: the contact force can only arise when two bodies are in contact and must vanish when bodies separate. The complementarity constraints can also be used to describe Coulomb friction, leading to nonlinear complementarity problems, which are difficult to solve. In [14], Anitescu proposed a relaxation to the complementarity problem by changing the non-penetration constraints into a quadratic dual cone constraint. While this relaxation introduces some mild non-physical artifacts [15], it obtains better computational properties and can be considered as the KKT optimality condition of a convex optimization problem [14]. In this paper, our ContactSDF model is also derived from the convex optimization-based contact model [14], [15]. But instead of focusing on an optimization-based time stepping, we propose using SDF representations to approximate the time-stepping prediction. This leads to a closed-form and differentiable contact model, which facilitates contact-rich model learning and optimization using existing tools [16], [17].

B. Model-based method for Dexterous Manipulation

The multi-modality and non-smoothness of complementarity-based models make them difficult to use in planning and control for manipulation. For systems with few contact modes, [11], [18] formulates contact planning as mixed-integer programs (MIPs). For contact-rich systems like dexterous manipulation, [10] proposes decoupling the planning horizon into small MIPs and using the alternating direction method of multipliers for parallel computation. [19] proposes reduced hybrid models that only capture the contact modes necessary for given tasks. Another strategy for contact-rich planning is to relax the complementarity constraints. For example, [4] relaxes the stiff complementary constraints with a slack variable and uses the interior-point method to solve the planning sequentially. Different from the existing MPC methods with implicit contact dynamics, since our ContactSDF is an explicit and differentiable model, planning with ContactSDF gets rid of combinatoric search and can be treated as a regular smooth optimization. This significantly improves the computational efficiency, making planning/control of dexterous manipulation faster.

C. Reinforcement Learning for Dexterous Manipulation

Reinforcement learning (RL) methods have achieved impressive results in dexterous manipulation tasks [20]–[22]. Model-free RL has the benefit of requiring less domain knowledge, but the cost is the millions or billions of environment data [23], making them difficult to be applied into hardware systems. Model-based RL [24] shows better data efficiency, but unstructured models may struggle to represent the non-smooth and multi-modality of contact interaction [1], [3], leading to lower performance compared to model-free approaches. The proposed method generally belongs to the model-based

category. Differently, the proposed ContactSDF model is a physical-based representation derived from classic multi-contact models. Due to the physics inductive bias, our method requires only thousands of training data to accomplish a contact-rich manipulation task.

D. Signed Distance Function Representation

Signed distance function (SDF) [25] has been widely used in computer vision for geometry learning and reconstructions [12], [26]. Due to its compact representation, SDF can be used for many tasks involving interpolation from sparse observations. The robotics community has started exploring its use in robot planning and manipulation. For example, [27] proposes utilizing neural SDF as a state transition model to facilitate manipulation. [28] formulates a neural grasp distance field as SDF to indicate the task completion distance. Our ContactSDF is also inspired by those works. But different from unconstructed SDF models learned from data, the proposed ContactSDF is physics-based, directly constructed from the multi-contact dynamics. Therefore, the SDFs in ContactSDF have direct physical correspondences: in collision detection routine, the SDF represents object geometry, and in time stepping prediction, the SDF approximates a projection to the feasible contact velocities satisfying contact constraints.

III. PRELIMINARY AND PROBLEM STATEMENT

A. Quasi-dynamic Multi-contact Model

We use quasi-dynamic models [29] to describe the equation of motion of a manipulation system state $\mathbf{q} := [\mathbf{q}_r, \mathbf{q}_o]$, including an actuated robot's position $\mathbf{q}_r \in \mathbb{R}^{n_r}$, unactuated object's position $\mathbf{q}_o \in \mathbb{R}^{n_o}$. Quasi-dynamic models have the benefits of simplicity by ignoring the inertial and Coriolis forces that are less significant in slow dexterous manipulation [6], [18], [30]. Specifically, consider a manipulation system with n_c potential contacts, which can happen between the object and robot or/and environment. Following [15], the cone complementary quasi-dynamic contact model for the system is

$$\begin{aligned} \mathbf{M}_o \mathbf{v}_o &= h m_o \mathbf{g} + \sum_{i=1}^{n_c} \mathbf{J}_{o,i}^\top \boldsymbol{\lambda}_i, \\ h \mathbf{K}_r (h \mathbf{v}_r - \mathbf{u}) &= h \boldsymbol{\tau}_r + \sum_{i=1}^{n_c} \mathbf{J}_{r,i}^\top \boldsymbol{\lambda}_i, \\ \mathcal{K}_i \ni \boldsymbol{\lambda}_i \perp \mathbf{J}_i \mathbf{v} + \frac{1}{h} \begin{bmatrix} \phi_i \\ 0 \\ 0 \end{bmatrix} &\in \mathcal{K}_i^*, \quad i = \{1, \dots, n_c\}. \end{aligned} \quad (1)$$

Here, h is the time step; \mathbf{M}_o is the regularized mass matrix of the object [6]; $\mathbf{v} := [\mathbf{v}_o, \mathbf{v}_r]$ is the system velocity stacking the object $\mathbf{v}_o \in \mathbb{R}^{n_o}$ and robot velocities $\mathbf{v}_r \in \mathbb{R}^{n_r}$; $\boldsymbol{\tau}_r \in \mathbb{R}^{n_r}$ is the non-contact force (e.g., gravity) applied to robot, and $m_o \mathbf{g}$ is the gravity force of the object with mass $m_o \in \mathbb{R}$ and gravity constant $\mathbf{g} \in \mathbb{R}^{n_o}$; $\boldsymbol{\lambda}_i := [\lambda_i^n, \boldsymbol{\lambda}_i^d] \in \mathbb{R}^3$ is the i -th contact impulse, with contact normal $\lambda_i^n \in \mathbb{R}$ and friction component $\boldsymbol{\lambda}_i^d \in \mathbb{R}^2$; ϕ_i is the signed distance at contact i ; the object's and robot's contact Jacobians are $\mathbf{J}_{o,i} := [\mathbf{J}_{o,i}^n; \mathbf{J}_{o,i}^d]$ and $\mathbf{J}_{r,i} := [\mathbf{J}_{r,i}^n; \mathbf{J}_{r,i}^d]$, respectively. The contact distance and Jacobians are computed by a collision detection (discussed later) for the system's current position $\mathbf{q} := (\mathbf{q}_o, \mathbf{q}_r)$.

The second equation in (1) follows [15], [31] and considers the actuated robot is in impedance control and can be treated as a ‘spring-like’ model with the stiffness matrix $\mathbf{K}_r \in \mathbb{R}^{n_r \times n_r}$. The robot input $\mathbf{u} \in \mathbb{R}^{n_r}$ is the desired position displacement. The third equation in (1) is the constraint between contact impulse and system motion, following Anitescu’s cone complementarity model [14]. Here, $\mathbf{J}_i := [\mathbf{J}_{o,i}, \mathbf{J}_{r,i}]$, \mathcal{K}_i is the Coulomb frictional cone, $\mathcal{K}_i := \{\boldsymbol{\lambda}_i \in \mathbb{R}^3 \mid \mu_i \lambda_i^n \geq \|\boldsymbol{\lambda}_i^d\|\}$; and \mathcal{K}_i^* is the dual cone of \mathcal{K}_i .

The work [14] shows that (1) is the KKT optimality conditions for the following second-order cone program (SOCP):

$$\begin{aligned} \min_{\mathbf{v}} \quad & \frac{h^2}{2} \mathbf{v}^\top \mathbf{Q} \mathbf{v} - h \mathbf{v}^\top \mathbf{b}(\mathbf{u}) \\ \text{subject to} \quad & \mathbf{J}_i \mathbf{v} + \frac{1}{h} \begin{bmatrix} \phi_i \\ 0 \\ 0 \end{bmatrix} \in \mathcal{K}_i^*, \quad i \in \{1 \dots n_c\}, \end{aligned} \quad (2)$$

where

$$\mathbf{Q} := \begin{bmatrix} \mathbf{M}_o/h^2 & \mathbf{0} \\ \mathbf{0} & \mathbf{K}_r \end{bmatrix}, \quad \mathbf{b}(\mathbf{u}) := \begin{bmatrix} m_o \mathbf{g} \\ \mathbf{K}_r \mathbf{u} + \boldsymbol{\tau}_r \end{bmatrix}. \quad (3)$$

One can further simplify (2) by approximating its second-order dual cone using a polyhedral cone [8]. Specifically, for contact i , one can use unit vectors $\{\mathbf{d}_{i,1}, \mathbf{d}_{i,2}, \dots, \mathbf{d}_{i,n_d}\}$ to symmetrically span the contact tangential plane [7], leading to the following linearized dual cone constraint

$$\mathbf{J}_i^n \mathbf{v} + \frac{\phi_i}{h} \geq \mu_i \mathbf{J}_{i,j}^d \mathbf{v}, \quad j \in \{1 \dots n_d\}, \quad (4)$$

where $\mathbf{J}_i^n := [\mathbf{J}_{o,i}^n, \mathbf{J}_{r,i}^n]$ is the system Jacobian to the contact normal, $\mathbf{J}_{i,j}^d := [\mathbf{J}_{o,i,j}^d, \mathbf{J}_{r,i,j}^d]$ is the system Jacobian to the unit directional vector \mathbf{d}_j in the tangential space. Hence, (2) can be simplified as a quadratic program (QP):

$$\begin{aligned} \min_{\mathbf{v}} \quad & \frac{1}{2} h^2 \mathbf{v}^\top \mathbf{Q} \mathbf{v} - h \mathbf{b}^\top \mathbf{v} \\ \text{s.t.} \quad & \mathbf{J}_{i,j} \mathbf{v} + \frac{\phi_i}{h} \geq 0, \quad i \in \{1 \dots n_c\}, \quad j \in \{1 \dots n_d\}, \end{aligned} \quad (5)$$

with $\mathbf{J}_{i,j}$ is defined as follows

$$\mathbf{J}_{i,j} := \mathbf{J}_i^n - \mu_i \mathbf{J}_{i,j}^d. \quad (6)$$

In a time-stepping prediction, $\mathbf{J}_{i,j}$ is calculated at the system’s current state \mathbf{q} from a collision detection routine. The solution \mathbf{v}^+ to (14) will be used to integrate from \mathbf{q} to the next \mathbf{q}^+ , i.e., $\mathbf{q}^+ := \mathbf{q} + h \mathbf{v}^+$, where “+” involves quaternion integration.

B. Model Predictive Control

Model predictive control (MPC) can be formulated as

$$\begin{aligned} \min_{\mathbf{u}_{0:T-1}} \quad & \sum_{t=0}^{T-1} c_t(\mathbf{q}_t, \mathbf{u}_t) + c_T(\mathbf{q}_T) \\ \text{s.t.} \quad & \mathbf{q}_{t+1} = \mathbf{f}(\mathbf{q}_t, \mathbf{u}_t), \quad t = 0, \dots, T-1, \quad \text{given } \mathbf{q}_0 \end{aligned} \quad (7)$$

where dynamic model $\mathbf{f}(\cdot)$ predicts future states of a system. Given initial \mathbf{q}_0 , (7) is solved for the optimal input sequence $\mathbf{u}_{0:T-1}^*(\mathbf{x}_0)$ over a prediction horizon T , by minimizing the path $c_t(\cdot)$ and final cost $c_T(\cdot)$. For a real system, the MPC controller is implemented in a receding horizon. Specifically, at rollout step k , the real system state is $\mathbf{q}_k^{\text{real}}$, and the MPC controller sets $\mathbf{q}_0 = \mathbf{q}_k^{\text{real}}$ and solves (7). Only the first optimal

input $\mathbf{u}_0^*(\mathbf{q}_k^{\text{real}})$ is applied to the real system, evolving the real system to the next state $\mathbf{q}_{k+1}^{\text{real}}$. This receding horizon process repeats and creates a closed-loop control effect, i.e., feedback from real system state $\mathbf{q}_k^{\text{real}}$ to control input \mathbf{u}_0^* .

C. Problem Statement

In MPC for contact-rich manipulation system, at rollout step k with system state $\mathbf{q}_k^{\text{real}}$, there are two routines inside MPC:

- *Collision detection routine*, which is to identify all potential contacts at $\mathbf{q}_k^{\text{real}}$. This routine returns contact distance ϕ_i and contact Jacobians $\mathbf{J}_{i,j}$ required in (5).
- *Time-stepping prediction routine*, which is to predict the future system states using the optimization-based quasi-dynamic model (5) given initial $\mathbf{q}_0 = \mathbf{q}_k^{\text{real}}$.

While both routines can be solved by existing tools, such as mature collision detection algorithms [32], [33], and quadratic programming solvers [34], [35]. However, each routine will create an optimization layer inside the MPC optimization (7); that is, the dynamic model \mathbf{f} includes two optimization layers. As a result, (7) is a multi-level optimization problem, creating challenges in computation and achieving real-time control.

In the following paper, we will show that each of the above routines can be replaced with an SDF, and thus, collision detection and time-stepping prediction can be approximated with an explicit, differentiable model \mathbf{f} , referred to as *ContactSDF* in the sequel, eliminating the needs of solving multi optimizations. Consequently, contact-rich MPC (7) can be solved efficiently with any trajectory optimization or MPCsolver [17].

IV. CONTACTSDF MODEL

We propose ContactSDF, which includes a **C-SDF** to approximate the collision detection and a **D-SDF** to approximate the time-stepping prediction in contact-rich manipulation systems.

A. C-SDF: Collision Detection SDF

We assume the geometry of an object in a manipulation system is given and convex, as required in many collision detection algorithms [33], [36]–[38]. The object geometry can be represented by a set of supporting planes [12]

$$\mathcal{G} = \{\mathbf{x} \mid \mathbf{n}_i^\top \mathbf{x} + b_i \leq 0, \quad i = 1, 2, \dots, I\}, \quad (8)$$

each parameterized by its unit normal vector $\mathbf{n}_i \in \mathbb{R}^3$ and offset $b_i \in \mathbb{R}$. Note that this supporting plane representation for object geometry can be obtained from depth data integration [39], [40], or learned from raw sensor data [12], [41], [42].

For collision detection in a manipulation system, we take an object-centric perspective. The collision detection is to calculate contact distance $\phi_{\mathcal{G}}(\mathbf{x}_{\text{query}})$ between a query point $\mathbf{x}_{\text{query}} \in \mathbb{R}^3$ to object \mathcal{G} :

$$\phi_{\mathcal{G}}(\mathbf{x}_{\text{query}}) := \min_{\mathbf{x} \in \mathcal{G}} \|\mathbf{x} - \mathbf{x}_{\text{query}}\|_2. \quad (9)$$

Here, a query point $\mathbf{x}_{\text{query}}$ can be taken from the surfaces of a robot or environment (e.g., ground). The distance becomes zero when the query point is inside the object (contact or penetration). $\phi_{\mathcal{G}}(\mathbf{x}_{\text{query}})$ in (9) can be considered as a truncated SDF for the object geometry representation \mathcal{G} . Getting $\phi_{\mathcal{G}}(\mathbf{x}_{\text{query}})$ requires

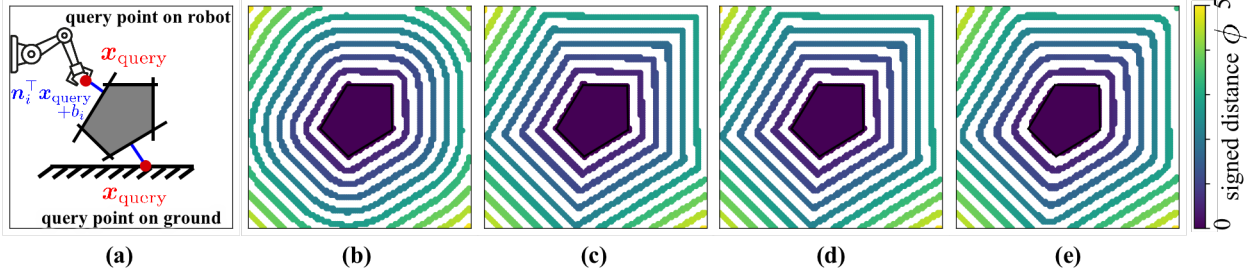


Fig. 2: 2D contact detection example. (a) Collision detection in a manipulation system can be viewed as a distance query to a convex object, where query points are taken from the robot and environment. (b) The truth distance field $\phi_{\mathcal{G}}(\mathbf{x}_{\text{query}})$ in (9) for the object. (c) Distance field approximated by (10). (d) The $\mathbf{C}\text{-SDF}_{\mathcal{G}}$ distance field (11) with large σ . (e) The $\mathbf{C}\text{-SDF}_{\mathcal{G}}$ distance field (11) with small σ .

solving an optimization. In the following, we will provide an SDF for fast approximation of (9), inspired by [12].

To motivate, we give a 2D example in Fig. 2. In Fig. 2(a), given a point $\mathbf{x}_{\text{query}}$ (on robot or ground) and a polytope object \mathcal{G} , the true contact distance field $\phi(\mathbf{x}_{\text{query}})$ in (9) is shown in Fig. 2(b). One can note that the signed distance between the $\mathbf{x}_{\text{query}}$ to each plane (\mathbf{n}_i, b_i) can be calculated as $\mathbf{n}_i^{\top} \mathbf{x}_{\text{query}} + b_i$. Thus, with large number I of supporting planes in \mathcal{G} , we can approximate $\phi_{\mathcal{G}}(\mathbf{x}_{\text{query}})$ in (9) using max function [12],

$$\phi_{\mathcal{G}}(\mathbf{x}_{\text{query}}) \approx \max\left(0, \max_{i=1,2,\dots,I} \{\mathbf{n}_i^{\top} \mathbf{x}_{\text{query}} + b_i\}\right), \quad (10)$$

as in Fig. 2(c). To facilitate the differentiability of (10), we apply LogSumExp (**LSE**) function to replace the inner and outer max operations, as used in [12]. This yields

$$\phi_{\mathcal{G}}(\mathbf{x}_{\text{query}}) \approx \frac{1}{\sigma} \underbrace{\mathbf{LSE} \left\{ 0, \mathbf{LSE} \left\{ \sigma(\mathbf{n}_i^{\top} \mathbf{x}_{\text{query}} + b_i), i=1, \dots, I \right\} \right\}}_{:=\mathbf{C}\text{-SDF}_{\mathcal{G}}(\mathbf{x}_{\text{query}})}. \quad (11)$$

Here, **LSE**(\cdot) operator is defined as

$$\mathbf{LSE}\{z_1, z_2, \dots, z_n\} = \log \sum_{i=1}^n \exp(z_i). \quad (12)$$

The hyperparameter σ in (11) is to control the approximation accuracy to max operation: the larger σ is, the closer (11) is to (10). Fig. 2 (d), (e) shows the distance fields of $\mathbf{C}\text{-SDF}_{\mathcal{G}}(\mathbf{x}_{\text{query}})$ with different choices of σ .

With $\mathbf{C}\text{-SDF}_{\mathcal{G}}(\mathbf{x}_{\text{query}})$ in (10) approximating $\phi_{\mathcal{G}}(\mathbf{x}_{\text{query}})$ in (9), the $\mathbf{x}_{\text{query}}$'s closest point \mathbf{x}^* on object \mathcal{G} , which is the solution to (9), can be retrieved by

$$\mathbf{x}^*(\mathbf{x}_{\text{query}}) = \mathbf{x}_{\text{query}} - \mathbf{C}\text{-SDF}_{\mathcal{G}}(\mathbf{x}_{\text{query}}) \nabla_{\mathbf{x}} \mathbf{C}\text{-SDF}_{\mathcal{G}}(\mathbf{x}_{\text{query}}). \quad (13)$$

Intuitively, $\nabla_{\mathbf{x}} \mathbf{C}\text{-SDF}_{\mathcal{G}}(\mathbf{x})$ is an approximate unit directional vector to the nearest point \mathbf{x}^* on \mathcal{G} , and $\mathbf{C}\text{-SDF}_{\mathcal{G}}(\mathbf{x}_{\text{query}})$ is the corresponding distance to \mathbf{x}^* . (13) provides an explicit differentiable alternative to collision detection (10). With the above approximated contact distance $\phi(\mathbf{x}_{\text{query}})$ and its on-object closest point $\mathbf{x}^*(\mathbf{x}_{\text{query}})$, contact Jacobian $\mathbf{J}_{i,j}$ required in (5) can be computed using differential kinematics [43].

B. $\mathbf{D}\text{-SDF}$: Time-Stepping Prediction SDF

We next show the optimization-based time-stepping model (2) can also be approximated by an SDF. First, we equivalently reformulate the time-stepping model (2) into the following

$$\begin{aligned} \min_{\mathbf{v}} \quad & \|h\mathbf{Q}^{\frac{1}{2}}\mathbf{v} - \mathbf{Q}^{-\frac{1}{2}}\mathbf{b}(\mathbf{u})\|_2 \\ \text{s.t.} \quad & \frac{\phi_i}{h} + \mathbf{J}_{i,j}(\mathbf{q})\mathbf{v} \geq 0, \quad i \in \{1\dots n_c\}, j \in \{1\dots n_d\}. \end{aligned} \quad (14)$$

Here contact Jacobian $\mathbf{J}_{i,j}$ and distance ϕ_i is obtained in $\mathbf{C}\text{-SDF}$ collision detection at system state \mathbf{q} . If one defines

$$\begin{aligned} \text{new variable} \quad & \mathbf{z} := h\mathbf{Q}^{\frac{1}{2}}\mathbf{v}, \\ \text{and new query point} \quad & \mathbf{z}_{\text{query}} := \mathbf{Q}^{-\frac{1}{2}}\mathbf{b}(\mathbf{u}), \end{aligned} \quad (15)$$

then the dual cone constraints in (14) can be re-written as

$$\mathcal{C}(\mathbf{q}) := \left\{ \mathbf{z} \mid \mathbf{n}_{i,j}^{\top} \mathbf{z} + b_{i,j} \leq 0, \quad \begin{matrix} i \in \{1\dots n_c\} \\ j \in \{1\dots n_d\} \end{matrix} \right\}. \quad (16)$$

with

$$\mathbf{n}_{i,j} := -\frac{\mathbf{Q}^{-\frac{1}{2}}\mathbf{J}_{i,j}^{\top}}{\|\mathbf{Q}^{-\frac{1}{2}}\mathbf{J}_{i,j}^{\top}\|}, \quad b_{i,j} := -\frac{\phi_i}{\|\mathbf{Q}^{-\frac{1}{2}}\mathbf{J}_{i,j}^{\top}\|}. \quad (17)$$

Since $\mathcal{C}(\mathbf{q})$ is state-dependent, we here explicitly write its dependence. With the above change of variable, the optimization-based time-stepping model (14) equivalently becomes

$$\phi_{\mathcal{C}(\mathbf{q})}(\mathbf{z}_{\text{query}}) = \min_{\mathbf{z} \in \mathcal{C}(\mathbf{q})} \|\mathbf{z} - \mathbf{z}_{\text{query}}\|_2. \quad (18)$$

The above (18) can be thought of as a collision detection problem in the \mathbf{z} -space (image of \mathbf{v} space) given $\mathbf{z}_{\text{query}} = \mathbf{Q}^{-\frac{1}{2}}\mathbf{b}(\mathbf{u})$. Thus, similar to (11), one can define

$$\mathbf{D}\text{-SDF}_{\mathcal{C}(\mathbf{q})}(\mathbf{z}_{\text{query}}) := \frac{1}{\sigma} \mathbf{LSE} \left(0, \mathbf{LSE} \left\{ \sigma(\mathbf{n}_{i,j}^{\top} \mathbf{z}_{\text{query}} + b_{i,j}), i \in \{1\dots n_c\}, j \in \{1\dots n_d\} \right\} \right) \quad (19)$$

to approximate $\phi_{\mathcal{C}(\mathbf{q})}(\mathbf{z}_{\text{query}})$ in (18). Further, one can approximate the optimal solution \mathbf{z}^+ to (18) using

$$\mathbf{z}^+ = \mathbf{z}_{\text{query}} - \mathbf{D}\text{-SDF}_{\mathcal{C}(\mathbf{q})}(\mathbf{z}_{\text{query}}) \nabla_{\mathbf{z}} \mathbf{D}\text{-SDF}_{\mathcal{C}(\mathbf{q})}(\mathbf{z}_{\text{query}}). \quad (20)$$

Note that \mathbf{z}^+ is in the \mathbf{z} -space. Recall definition (15), we map \mathbf{z}^+ back to the \mathbf{v} -space by $\mathbf{v}^+ = \frac{1}{h}\mathbf{Q}^{-\frac{1}{2}}\mathbf{z}^+$.

In sum, with (15) and (20) one can finally write the explicit **D-SDF** time-stepping model, directly mapping from the current state \mathbf{q} and input \mathbf{u} to the next velocity \mathbf{v}^+ , as

$$\mathbf{v}^+ = \frac{1}{h}\mathbf{Q}^{-1}\mathbf{b}(\mathbf{u}) - \frac{1}{h}\mathbf{Q}^{-\frac{1}{2}}\left(\mathbf{D-SDF}_{\mathcal{C}(\mathbf{q})}\left(\mathbf{Q}^{-\frac{1}{2}}\mathbf{b}(\mathbf{u})\right)\right) \\ \nabla_{\mathbf{z}}\mathbf{D-SDF}_{\mathcal{C}(\mathbf{q})}\left(\mathbf{Q}^{-\frac{1}{2}}\mathbf{b}(\mathbf{u})\right). \quad (21)$$

The next state \mathbf{q}^+ is then obtained by integrating \mathbf{q} with \mathbf{v}^+ . On (21), we make the following comments.

The first term $\frac{1}{h}\mathbf{Q}^{-1}\mathbf{b}(\mathbf{u})$ in (21) is the predicted velocity by non-contact force (e.g., gravity or input). The second term is a contact-related term. Recalling **D-SDF** in (19), calculating this term requires comparing the distance between the query $\mathbf{Q}^{-\frac{1}{2}}\mathbf{b}(\mathbf{u})$ with all faces of the polyhedron dual cones (18). Importantly, (20) provides an explicit prediction model, bypassing optimization-based time stepping prediction in classic complementarity-based contact models.

Different from **C-SDF** $_{\mathcal{G}}$ (11) where one can arbitrarily increase the number of supporting planes in \mathcal{G} to control the collision detection accuracy [12], The dual cone constraint $\mathcal{C}(\mathbf{q})$ in the time-stepping **D-SDF** $_{\mathcal{C}(\mathbf{q})}$ cannot be arbitrarily altered as it determined by the results of collision detection at system state \mathbf{q} . Therefore, using the **D-SDF** (21) to approximate the true dynamics may introduce some model approximation error. Thankfully, differentiability of **D-SDF** makes it easy to use real system data to find good model parameters that minimizes the model gap, as we will present in the next section.

V. CONTACTSDF-MPC AND **D-SDF** LEARNING

A. ContactSDF-MPC

With collision detection **C-SDF** (11), and time stepping prediction **D-SDF** (21), we present the ContactSDF-MPC:

$$\min_{\mathbf{u}_{0:T-1} \in [\mathbf{u}_{lb}, \mathbf{u}_{ub}]} \sum_{t=0}^{T-1} c_t(\mathbf{q}_t, \mathbf{u}_t) + c_T(\mathbf{q}_T) \\ \text{subject to } \mathbf{q}_{t+1} = \mathbf{q}_t + h\mathbf{v}_t^+, \quad t = 0, 1, \dots, T \\ \mathbf{v}_t^+ \text{ is solved from } \mathbf{D-SDF}_{\mathcal{C}(\mathbf{q}_0)} \text{ in (21),} \\ \mathcal{C}(\mathbf{q}_0) \text{ is obtained from } \mathbf{C-SDF}_{\mathcal{G}} \text{ in (11),} \\ \text{given } \mathbf{q}_0. \quad (22)$$

Note $\mathcal{C}(\mathbf{q}_t)$ is supposed to be computed at predicted \mathbf{q}_t , $t = 0, \dots, T$. However, to reduce the computational complexity, we assume $\mathcal{C}(\mathbf{q}_t)$ is fixed in the relatively short MPC prediction horizon T , i.e., we assume $\mathcal{C}(\mathbf{q}_t) \approx \mathcal{C}(\mathbf{q}_0)$ within MPC prediction. It should be noted that since both **C-SDF** and **D-SDF** are explicit and differentiable, ContactSDF-MPC is capable of handling the time-varying $\mathcal{C}(\mathbf{q}_t)$ in the MPC prediction horizon.

B. Learning **D-SDF** Model with On-MPC Data

To improve the accuracy of **D-SDF** in time-stepping prediction, we propose using the on-MPC data to learn **D-SDF** model, based on our prior work [19]. By learning **D-SDF** model, we mean learning all model parameters of **D-SDF**, including

$$\boldsymbol{\theta} := \{\mathbf{M}_o, \mathbf{K}_r, m_o, \mu, \sigma\}, \quad (23)$$

The learning loss is defined as the prediction loss

$$\mathcal{L}(\boldsymbol{\theta}, \mathcal{D}_{\text{on-MPC}}) = \sum_{(\mathbf{q}_k^{\text{real}}, \mathbf{u}_k, \mathbf{q}_{k+1}^{\text{real}}) \in \mathcal{D}} \|\mathbf{q}_{k+1}(\boldsymbol{\theta}) - \mathbf{q}_{k+1}^{\text{real}}\|^2. \quad (24)$$

where \mathbf{q}_{k+1} is the predicted next state from **D-SDF** given $(\mathbf{q}_k^{\text{real}}, \mathbf{u}_k)$. Since the **D-SDF** is differentiable, the model can be updated using any gradient-based methods.

The pipeline of **D-SDF** learning with the on-MPC data follows our prior work [19], shown in Fig. 3. It includes two alternative steps: (1) ContactSDF-MPC rollouts on the real system and collects the on-MPC data into a buffer $\mathcal{D}_{\text{on-MPC}}$, and (2) **D-SDF** is updated using data in $\mathcal{D}_{\text{on-MPC}}$.

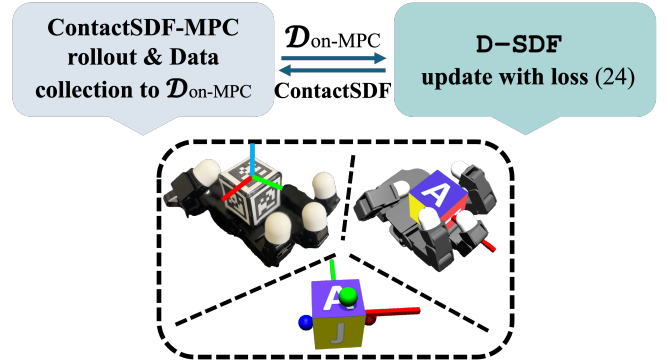


Fig. 3: Pipeline of learning **D-SDF** from on-MPC data [19].

VI. SIMULATED EXPERIMENTS

In this section, we evaluate the ContactSDF-MPC in two contact-rich manipulation environments: *three-ball manipulation* and *Allegro hand on-palm reorientation*, both with different objects. The environments are built in MuJoCo physics simulator [44]. In each task, we first learn ContactSDF (**D-SDF** model) using on-MPC data and then evaluate the ContactSDF MPC. Baseline comparison is also provided. All experiments are run on a PC with an Intel i9-13900K chip. The MPC optimization (22) is solved using CasADi [17]. The codes are available in [github](#).

A. Three-Ball Manipulation

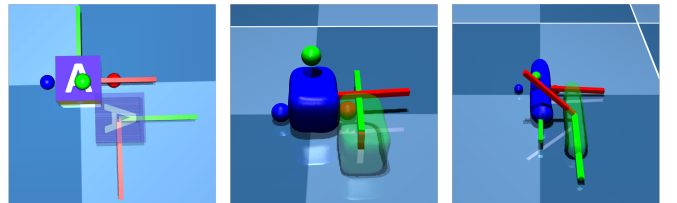


Fig. 4: Three-ball manipulation with cube (left), foambrick (middle), stick (right). Target poses are shown in transparency. The red and green bars are only used to visualize the x and y axis of object frame, respectively.

1) *Task Setup*: As in Fig. 4, the three-ball manipulation involves three balls (red, green, and blue), each with 3 DoFs actuated by a low-level position controller with gravity

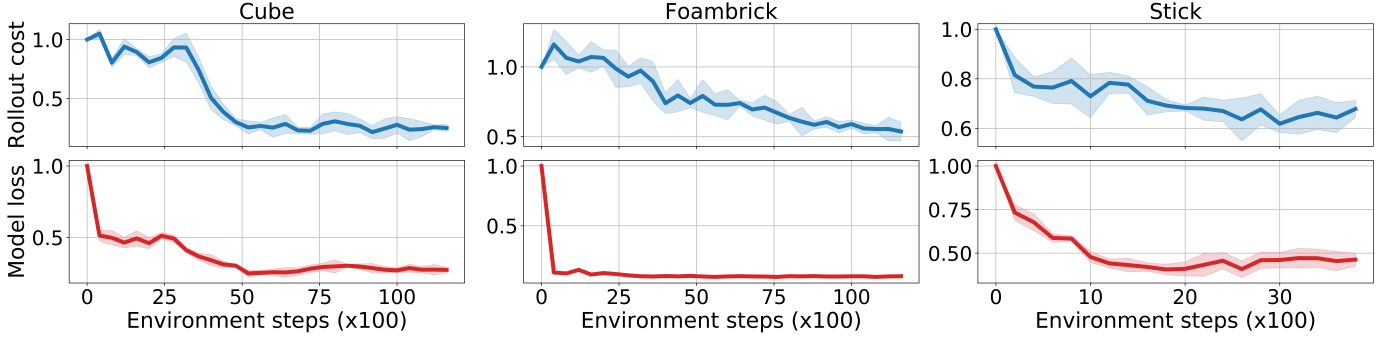


Fig. 5: Learning **D-SDF** with on-MPC data in the three-ball manipulation tasks. The first and second rows show the normalized accumulated cost of environment rollout, evaluated by c_T (25), and normalized model prediction loss (24) along with the learning steps. Each plot is based on five learning trials, showing the mean and 95% confidential intervals.

TABLE I: Target object poses in the three-ball manipulation tasks

Tasks	Cube/Foambrick	Stick
(x,y) position [m]	$\{(\pm 0.05, \pm 0.05)\}$	$\{(\pm 0.05, \pm 0.05)\}$
z-axis rotation [rad]	$\{0, \pm \frac{\pi}{4}, \pm \frac{\pi}{2}\}$	$\{0, \pm \frac{\pi}{4}, \pm \frac{\pi}{2}\}$
y-axis flipping [rad]	$\{\pm \frac{\pi}{2}\}$	$\{\frac{3}{4}\pi, \pi\}$

compensation, and a 6-DoF object on frictional ground. Three objects are used: cube, foambrick, and stick, with their geometry given, and their (length, width, height) sizes are (56,56,56), (52,75,47), and (130,35,30), respectively. The task goals are that three balls translate, rotate, and/or flip an object from an initial pose (aligned with the world frame) to a random on-ground target (shown in transparency in Fig. 4). The object targets are given in Table. I, where each target object pose is a combination of a target position and a target rotation (z-axis yaw rotation or y-axis flipping).

2) *ContactSDF setting*: The system state \mathbf{q} involves object pose $\mathbf{q}_o \in \mathbb{R}^7$ and the positions of three balls $\mathbf{q}_r \in \mathbb{R}^9$; the control input $\mathbf{u} \in \mathbb{R}^9$ is the desired position displacement of three balls, which is sent to the low-level position controller. The time interval in **D-SDF** is set to $h = 0.1s$. Other parameters (23) in **D-SDF** will be learned using on-MPC data.

In collision detection **C-SDF**, for contacts between the object and three balls, the balls are considered as query points $\mathbf{x}_{\text{query}}$. For contact between the object and ground, the query points are the ground points, which are evenly sampled from the ground projection area of the object (like Fig. 2(a)). For each object, its supporting plane representation \mathcal{G} in (8) is directly generated from its mesh model or point cloud data. Given all queried distances $\phi_{\mathcal{G}}(\mathbf{x}_{\text{query}})$ in (9), we set a threshold to remove query points of larger $\phi_{\mathcal{G}}$ s for which contact is not possible. The frictional cone is linearized with $n_d = 4$.

In ContactSDF-MPC (22), $T=4$, and control bounds are $\mathbf{u}_{\text{lb}} = -0.01$ and $\mathbf{u}_{\text{ub}} = 0.01$. The path and final costs are

$$\begin{aligned} c_t(\mathbf{q}, \mathbf{u}) &= \omega_c c_{\text{contact}} + \omega_g c_{\text{grasp}} + \omega_u \|\mathbf{u}\|^2 \\ c_T(\mathbf{q}) &= \omega_p \|\mathbf{p}_o - \mathbf{p}_o^{\text{target}}\|^2 + \omega_q (1 - (\mathbf{q}_o^T \mathbf{q}_o^{\text{target}})^2). \end{aligned} \quad (25)$$

respectively. The above path cost $c_t(\mathbf{q}, \mathbf{u})$ has three terms: (i)

The contact cost term, defined as

$$c_{\text{contact}} = \sum_{i=0}^2 \|\mathbf{p}_{\text{ball},i} - \mathbf{p}_o\|^2, \quad (26)$$

is to encourage the contact between the three balls and object. (ii) The grasp cost term, defined as

$$c_{\text{grasp}} = \|\mathbf{d}_0 + \mathbf{d}_1 + \mathbf{d}_2\|^2, \quad (27)$$

is to encourages a grasp closure by the three balls; Here, \mathbf{d}_i is a unit directional vector from object position \mathbf{p}_o to each ball position $\mathbf{q}_{\text{ball},i}$, $\mathbf{d}_i = \mathbf{R}_o^T (\mathbf{q}_{\text{ball},i} - \mathbf{p}_o) / \|(\mathbf{q}_{\text{ball},i} - \mathbf{p}_o)\|$, viewed in object frame \mathbf{R}_o . (iii) $\|\mathbf{u}\|^2$ is the control effort. The three cost terms are assigned with weights ω_c , ω_g , and ω_u , respectively. The final cost $c_T(\mathbf{q})$ defines the distance between the object pose ($\mathbf{p}_o, \mathbf{q}_o$) and target ($\mathbf{p}_o^{\text{target}}, \mathbf{q}_o^{\text{target}}$), with position and quaternion weights ω_p and ω_q , respectively. The cost weights $\{\omega_c, \omega_g, \omega_u, \omega_p, \omega_q\}$ are set (based on physical scale): $\{1, 0.1, 1, 10000, 1000\}$ for cube, $\{1, 0.1, 1, 10000, 5000\}$ for foambrick, and $\{1, 0.1, 1, 500, 100\}$ for stick.

3) *Results and Comparison*: Following the procedure in Fig. 3, we first learn the **D-SDF** model (i.e., parameter θ in (23)) with on-MPC data for each object manipulation. Here, we set the ContactSDF-MPC rollout length to $H = 100$. **D-SDF** is updated every 4 on-MPC rollout collections (i.e., every 400 environment steps). Each rollout is tasked with a target (position + rotation) uniformly sampled from Table I. We show the learning results in Fig. 5. The plots in Fig. 5 show that a **D-SDF** can be successfully learned with less than 5k environment steps. With the learned **D-SDF** model for each object, we next evaluate the ContactSDF-MPC.

In evaluation, we compare ContactSDF-MPC with the MPC that uses the optimization-based model (5). We refer to the latter as QPModel-MPC. To solve QPModel-MPC with existing solver [17], we replace the QP model (5) with its KKT conditions with a relaxation ϵ for complementarity conditions, similar to [4]. The ContactSDF-MPC and QPModel-MPC share both the same cost functions (25) and the learned parameter θ . For each object, we run ContactSDF-MPC and QPModel-MPC for 7 trials, each trial with a different target sampled from in Table. I, and rollout length set to $H = 200$ for cube and $H = 300$ for foambrick and stick. The evaluation results

TABLE II: Comparison results for the three-ball manipulation tasks

Case	Terminal position error [mm]↓		Terminal orientation error [rad]↓		MPC solving cost [ms] ↑	
	ContactSDF-MPC	QPModel-MPC	ContactSDF-MPC	QPModel-MPC	ContactSDF-MPC	QPModel-MPC
Cube	13.62±3.14	26.11±28.24	0.11±0.11	0.24±0.35	31.77±9.13	80.76±14.19
Foambrick	8.93±2.31	8.59±3.17	0.24±0.02	0.19±0.05	24.95±8.00	51.64±15.81
Stick	22.06±5.90	30.54±8.72	0.26±0.19	0.37±0.22	52.81±5.99	91.94±10.56

The results of each object are reported using 7 random trials including 5 turning and 2 flipping targets. The position and orientation errors are computed at the last step of MPC rollout. The relaxation factor in QPModel-MPC is set $\epsilon=10^{-4}$ for best performance.

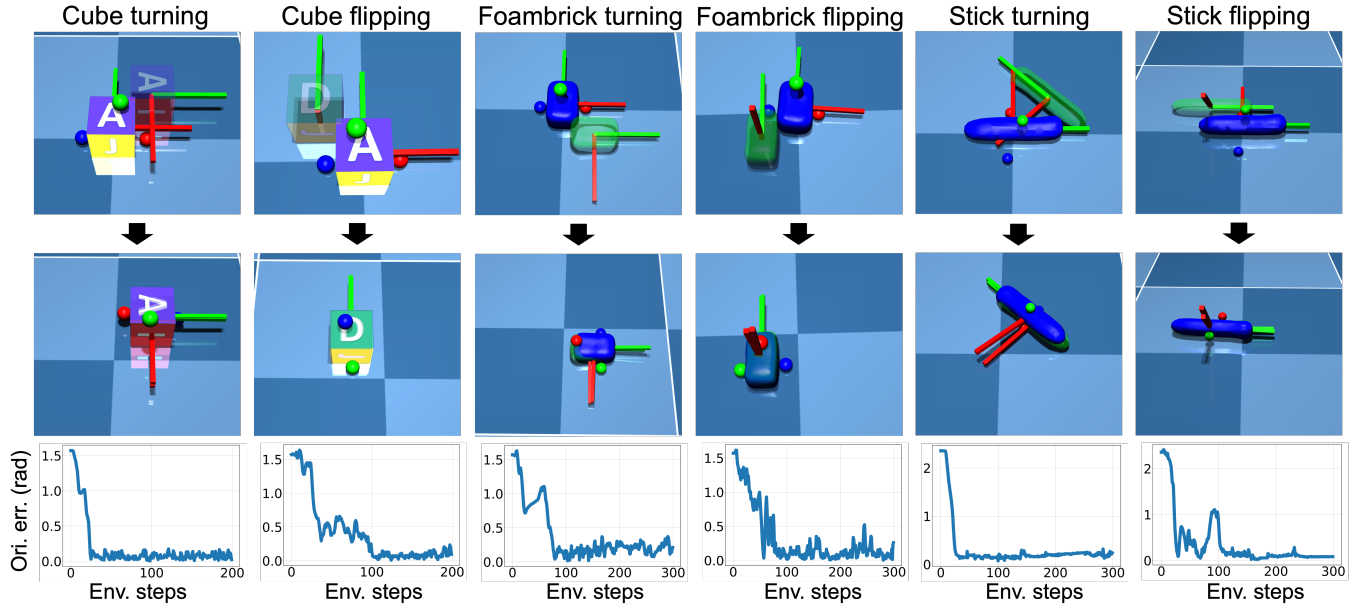


Fig. 6: Evaluation examples for ContactSDF-MPC in the three-ball manipulation tasks. We show a turning and flipping target case for each object. The first and the second rows show the initial and final scenes of a task, respectively. The third row plots the object orientation error over ContactSDF-MPC rollout steps.

are shown in Table II. As visualization examples, we show a turning and flipping task for each object in Fig. 6.

The results in Table II and Fig. 6 demonstrate ContactSDF-MPC achieves noticeably higher manipulation accuracy compared to QPModel-MPC under the same cost function and model parameters. Specifically, ContactSDF-MPC reduces average position error by 31.6% and orientation error by 24.9% across various tasks. Moreover, ContactSDF-MPC has a substantial optimization speed advantage, with MPC solving time being 103% faster on average than QPModel-MPC. This speed advantage is primarily due to the elimination of complementarity in ContactSDF.

B. Allegro Hand On-palm Reorientation

1) *Task Setup*: As in Fig. 8, the Allegro robotic hand has four 4-DoF fingers with the palm facing upward. We consider the on-palm object reorientation task with the three objects also used in the three-ball manipulation. The task involves reorienting objects from an initial orientation (identity pose) on the palm to given target orientations. We specifically consider the reorientation around the z-axis (yaw rotation), with the target given in Table III.

2) *ContactSDF Setting*: The system position $\mathbf{q} \in \mathbb{R}^{23}$, including the object pose $\mathbf{q}_o \in \mathbb{R}^7$ and robot (four fingers) joint

TABLE III: Targets in Allegro hand on-palm reorientation tasks

Target	Cube/Foambrick	Stick
z-axis (yaw) rotation	$\{\pm\frac{\pi}{4}, \pm\frac{\pi}{3}, \pm\frac{\pi}{2}\}$	$\{\pm 0.2\pi, \pm 0.25\pi, \pm 0.3\pi\}$

position $\mathbf{q}_r \in \mathbb{R}^{16}$. $\mathbf{u} \in \mathbb{R}^{16}$ is the desired joint displacement, which is sent to a low-level joint PD controller. The parameters θ (23) in **D-SDF** will be learned using on-MPC policy data.

In collision detection **C-SDF**, for the contact between fingers and the object, query points $\mathbf{x}_{\text{query}}$ spread across the surfaces of fingers as shown in Fig. 9; and for the contact between the object and palm, query points are sampled on the palm surface. Contact distances are then filtered to remove distant queries.

The setting of the ContactSDF-MPC (22) follows the three-ball manipulations. The cost functions are the same as (25), except that the grasp cost term is removed as it is not critical for on-palm orientation tasks. The cost weights $\{\omega_c, \omega_u, \omega_p, \omega_q\}$ are $\{0.5, 0.1, 1000, 10000\}$ for cube, $\{1, 0.2, 500, 5000\}$ for foambrick and $\{0.5, 0.2, 1000, 10000\}$ for stick.

3) *Results*: Similar to the procedure in the previous three-ball manipulation, all parameters θ (23) in the **D-SDF** are learned for the Allegro hand tasks. The MPC rollout length is set to $H = 100$ and the model is updated every four rollouts. In each rollout, the reorientation target is uniformly sampled

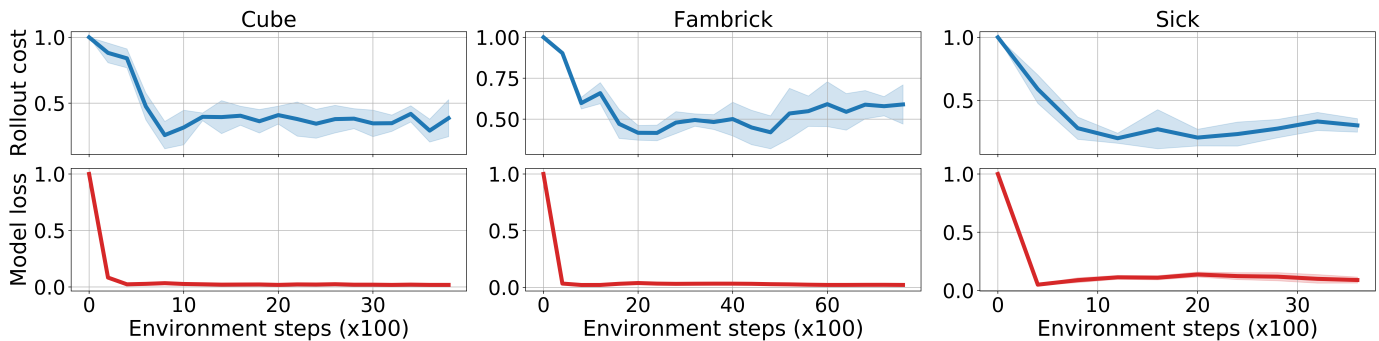


Fig. 7: Learning $\mathbf{D-SDF}$ with on-MPC data in the Allegro hand on-palm reorientation tasks. The first and second rows show the normalized accumulated cost of environment rollout, evaluated by c_T (25), and normalized model prediction loss (24) along with the learning steps. Each plot is based on five learning trials, showing the mean and 95% confidential intervals.

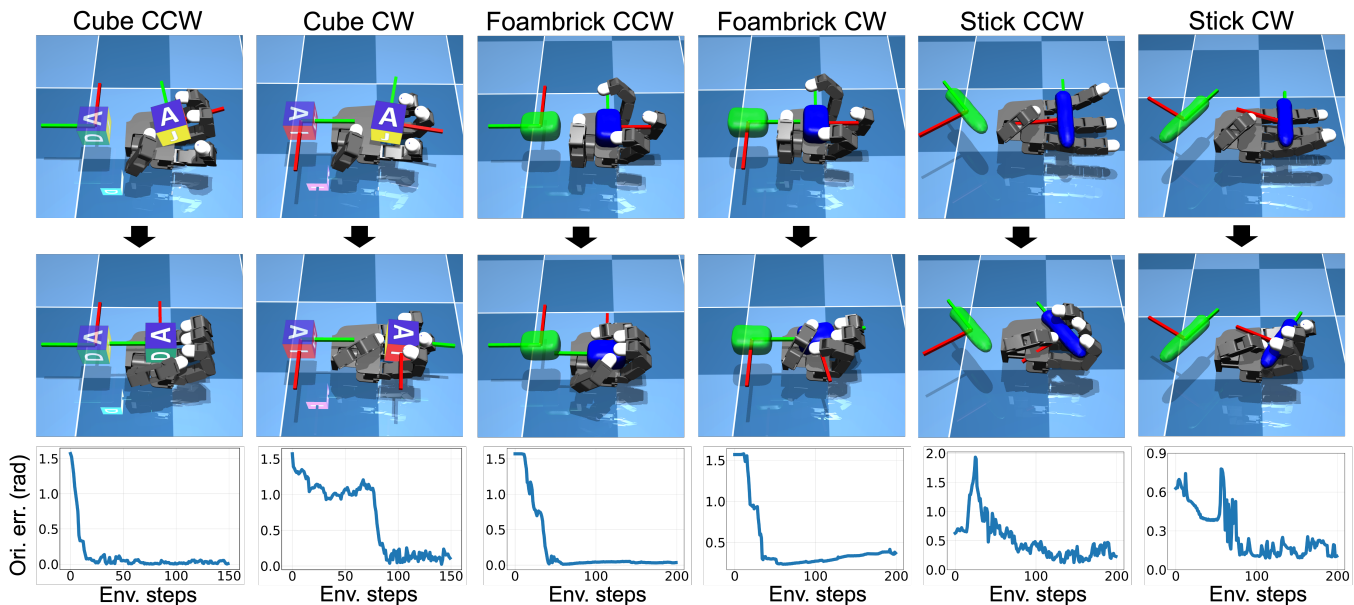


Fig. 8: Evaluation examples for ContactSDF-MPC in the three-ball manipulation tasks. We show a counterclockwise (CCW) and clockwise (CW) target for each object. The first and the second rows show the initial and final scenes of each task, respectively. The third row plots the object orientation error over ContactSDF-MPC rollout steps.

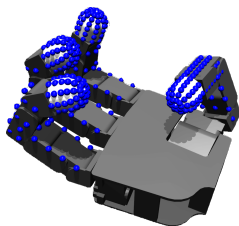


Fig. 9: Contact query point samples on four fingers.

from Table. III. The learning results are shown in Fig. 7.

TABLE IV: Evaluation performance of ContactSDF-MPC for Allegro In-hand reorientation tasks

Metrics	Cube	Foambrick	Stick
Terminal orientation err. (rad)	0.08 ± 0.06	0.17 ± 0.15	0.28 ± 0.21
MPC running frequency (Hz)	40.6 ± 17.1	40.3 ± 12.9	46.9 ± 15.3

With the learned $\mathbf{D-SDF}$, we evaluate the performance of ContactSDF-MPC. For each object, ContactSDF-MPC is evaluated for 6 trials, each with a different rotation target uniformly sampled from Table. III, rollout length set to $H = 150$ for cube and $H = 200$ for foambrick and stick. The evaluation results are listed in Table. IV. Fig. 8 visualizes some evaluation examples.

With the learning and evaluation results given above, we draw the following conclusions: (i) Fig. 7 shows the ContactSDF model converges quickly within about 2k environment steps. As the ContactSDF is built upon physics structures, with a few parameters to be learned. Thus, the learning is very data-efficient. (ii) Table. IV illustrates that the ContactSDF-MPC achieves high manipulation accuracy for the Allegro on-palm reorientation tasks: the average reorientation error is 0.08 rad for the cube, 0.17 rad for foambrick. For the stick, despite its non-equilibrium targets, it still accomplishes the rotating task with an averaged angle error of 0.28 rad. Examples in Fig. 8

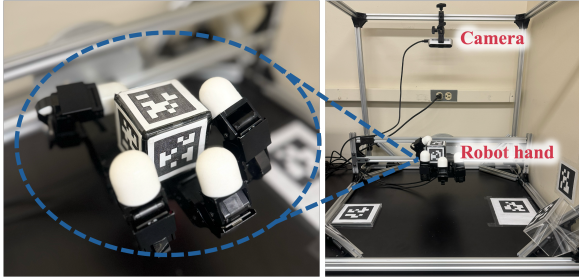


Fig. 10: Allegro hand (V4) hardware system.

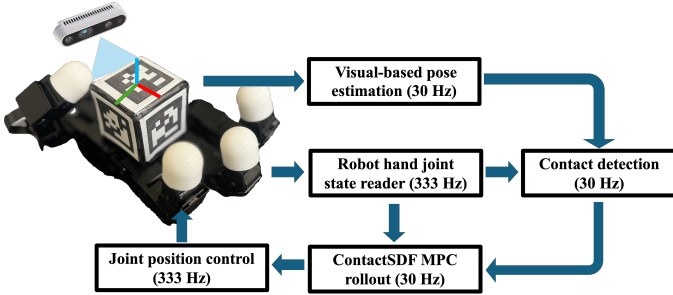


Fig. 11: System diagram for the hardware implementation. Different blocks indicate separate processes connected via arrows that indicate communication via ROS.

also illustrate the accuracy of the reorientation task. (iii) Table IV shows that the ContactSDF-MPC achieves a real-time speed for MPC of Allegro in-hand manipulation, and the average MPC running frequency is above 40 Hz.

VII. HARDWARE IN-HAND DEXTEROUS MANIPULATION

In this section, we evaluate the ContactSDF on a hardware Allegro Hand for on-palm reorientation tasks.

A. Hardware Implementation

The hardware Allegro hand system is shown in Fig. 10, and it has four 4-DoF fingers, each actuated by a low-level joint position PD controller running at a frequency of 333Hz. We use a cube object of ($56 \times 56 \times 56$ mm), with each face attached with an AprilTag [45] for vision-based pose (position and quaternion) estimation. We consider the reorientation of the cube in z -axis (yaw angle).

An RGB-D camera (Intel D435i RealSense), is used for the real-time pose estimation of the object using TagSLAM algorithm [46]. The system framework is depicted as Fig. 11. The object pose estimation has a frequency of 30 Hz. ROS [47] is used to implement the communication of different modules.

In contact detection **C-SDF**, the selection of contact query points follows that in our previous simulation experiments, i.e., the query points are selected from the surfaces of each finger (see Fig. 9) and palm. As shown in Fig. 11, we synchronize the vision-based object pose estimation with the **C-SDF** contact detection as the collision detection is pose-dependent.

In ContactSDF, the system state \mathbf{q} includes the joint position of all fingers $\mathbf{q}_r \in \mathbb{R}^{16}$, and cube pose $\mathbf{q}_o \in \mathbb{R}^7$. The robot input $\mathbf{u} \in \mathbb{R}^{16}$ is the desired finger joint displacement sent to the

finger lower-level PD controller. The model and ContactSDF-MPC (22) settings are given in Table V.

TABLE V: Parameters of hardware Allegro hand experiments

Parameter	Value
Time interval h in D-SDF	0.1 [s]
MPC prediction horizon T	3
Cost weights (25) $\{\omega_c, \omega_u, \omega_p, \omega_q\}$	$\{1, 0.2, 500, 5000\}$
ContactSDF-MPC control bounds	$\mathbf{u}_{lb} = -0.15$ and $\mathbf{u}_{ub} = 0.15$
Incremental sub-goal setting	current yaw angle $\pm 90^\circ$
ContactSDF-MPC rollout length H	100
$\mathcal{D}_{\text{buffer}}$ buffer size	400 [environment steps]

B. **D-SDF** Learning on Hardware on-MPC Data

Unlike in simulated experiments where one can conveniently reset the cube state during the learning, resetting the cube state on hardware has to be manual. To reduce the manual effort of cube resetting, our task goal in the learning stage is to continuously rotate the cube around the z -axis. We achieve this by incrementally setting sub-goals, each involving adding 90° (CCW) to the cube’s yaw angle at the end of the previous MPC rollout. Since four fingers have their mechanical limitation, when an MPC rollout ends, the fingers are reset to their initial joint positions. The finger joint reset operates independently from the algorithm’s planning and learning modules and will not be added to the data buffer.

We directly learn **D-SDF** from *scratch* using the hardware on-MPC data. The **D-SDF** is updated every four hardware MPC rollouts. Each rollout corresponds to an incremental sub-goal and has a length of 100 steps. The **D-SDF** learning results are shown in Fig. 12. Here, the upper panel is accumulated cost of the hardware rollouts, and the bottom panel is the model evaluation loss. The plots in Fig. (12) show that the ContactSDF model is efficiently learned with around 2k hardware steps.

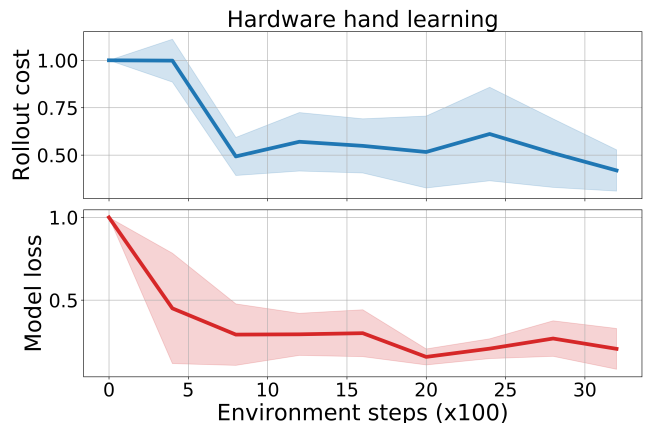


Fig. 12: Learning **D-SDF** from on-MPC hardware data for the Allegro hand continuous reorientation tasks. The first and second rows show the normalized accumulated cost of environment rollout (evaluated by c_T) and normalized model prediction loss, respectively, along with the learning steps. Note that the **D-SDF** updates every 400 environment steps.

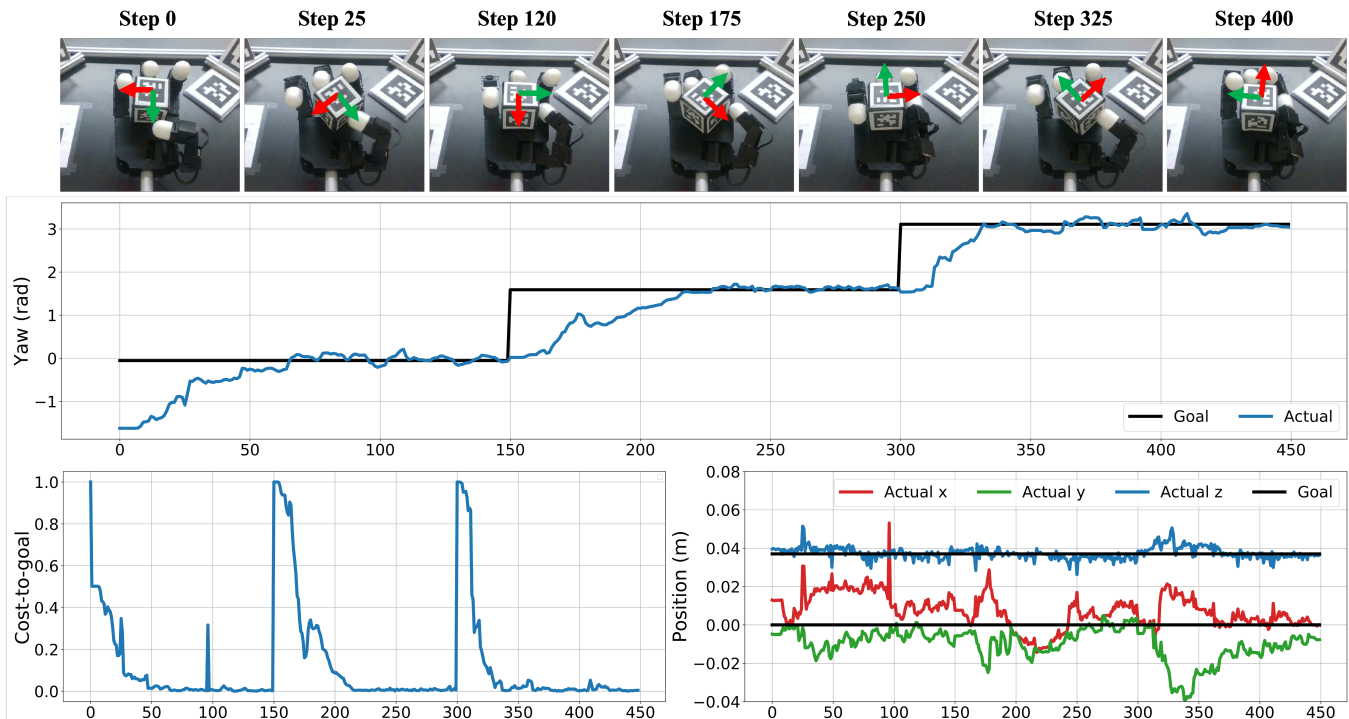


Fig. 13: Continuous reorientation task on hardware. The first row shows the snapshots of the system at different rollout steps. In the second row, the black line indicates the incremental yaw targets, and the blue line shows the actual yaw angle of the cube. The left panel in the third row shows the normalized cost-to-goal of the system, evaluated using the final cost $c_T(\cdot)$ in (25) at every rollout step; and the right panel show the cube position versus the rollout steps.

C. Evaluation of ContactSDF-MPC for Single Rotations

With the learned **D-SDF**, we evaluate the performance of ContactSDF-MPC for reorientation tasks given single 90° (CCW) or -90° (CW) rotation goals. For each direction, we perform 5 trials. In each trial, the cube is randomly placed around the palm center (Fig. 10), and we run ContactSDF-MPC for one rollout with length of $H = 100$. The evaluation results are reported in VI.

TABLE VI: Evaluation results for single orientation goals

	CCW	CW
Terminal orientation err. (rad)	0.11 ± 0.05	0.19 ± 0.15
MPC running frequency (Hz)	47.2 ± 12.8	49.5 ± 11.3

Results in Table. VI shows a high reorientation accuracy of ContactSDF-MPC for single rotation tasks. The average reorientation error is 0.15 rad for both rotation directions (CCW and CW). Importantly, the ContactSDF-MPC can run 50Hz on the hardware.

D. Evaluation of ContactSDF-MPC for Continuous Rotation

Next, we evaluate the ContactSDF-MPC for the *continuous* rotation of the cube without human resetting. Similar to the learning stage, the sub-goal is incremented by adding 90° to the cube yaw angle at the end of each ContactSDF-MPC rollout ($H = 150$ steps). Also when a MPC rollout ends, the fingers

are reset to their initial joint positions. Initially the cube the randomly placed on the palm.

The results are shown in Fig. 13. Here, the first row depicts the snapshots of the hardware system at different rollout steps, and the second row shows the trajectories of the incremental rotation target (black line) and actual cube yaw angle (blue line). As plotted, there are three incremental sub-goals; after each sub-goal is achieved at the end of an MPC rollout, the target cube angle is updated to the next by adding 90° . The blue line shows the yaw angle trajectory of the cube (from the visual perception). The left panel in the third row reports the normalized cost-to-goal of the system, evaluated using final cost $c_T(\cdot)$ in (25) at every rollout step. The right panel shows the x-y-z positions of the cube during the continuous task, where the black lines represent the target position. The ContactSDF-MPC can run at about 50 Hz. The entire continuous rotation task took approximately 15 seconds.

VIII. CONCLUSION AND FUTURE WORK

We proposed the ContactSDF, a differentiable model designed for efficient learning and control of contact-rich manipulation systems. By using signed distance functions to approximate both collision detection and time-stepping prediction, ContactSDF eliminates the hybrid and non-smooth routines in classic complementarity-based contact model formulation. ContactSDF can be readily integrated with existing learning and model-based control methods for efficiently solving dexterous manipulation. The effectiveness and efficiency of ContactSDF

for learning and control of dexterous manipulation tasks has been extensively demonstrated in both simulation and hardware experiments. Notably, results show that with around 2 minutes of learning on hardware, the ContactSDF achieves high-quality dexterous manipulation at a frequency of 30-60Hz.

There are several areas unexplored for the proposed ContactSDF model, such as jointly learning object geometry SDF $C-SDF_G$ and generalizing the hardware experiments to objects with more complicated geometries. We will explore those in our future work.

REFERENCES

- [1] Mihir Parmar, Mathew Halm, and Michael Posa. Fundamental challenges in deep learning for stiff contact dynamics. In *2021 IEEE/RSJ International Conference on Intelligent Robots and Systems (IROS)*, pages 5181–5188. IEEE, 2021.
- [2] Wanxin Jin, Alp Aydinoglu, Mathew Halm, and Michael Posa. Learning linear complementarity systems. *CoRR*, abs/2112.13284, 2021.
- [3] Samuel Pfrommer, Mathew Halm, and Michael Posa. Contactnets: Learning discontinuous contact dynamics with smooth, implicit representations. In *Conference on Robot Learning*, pages 2279–2291. PMLR, 2021.
- [4] Simon Le Cleac’h, Taylor A. Howell, Mac Schwager, and Zachary Manchester. Linear contact-implicit model-predictive control. *CoRR*, abs/2107.05616, 2021.
- [5] Alp Aydinoglu and Michael Posa. Real-time multi-contact model predictive control via admm. In *2022 International Conference on Robotics and Automation (ICRA)*, pages 3414–3421. IEEE, 2022.
- [6] Tao Pang, HJ Terry Suh, Lujie Yang, and Russ Tedrake. Global planning for contact-rich manipulation via local smoothing of quasi-dynamic contact models. *IEEE Transactions on Robotics*, 2023.
- [7] David Stewart and Jeffrey C Trinkle. An implicit time-stepping scheme for rigid body dynamics with coulumb friction. In *Proceedings 2000 ICRA. Millennium Conference. IEEE International Conference on Robotics and Automation. Symposia Proceedings (Cat. No. 00CH37065)*, volume 1, pages 162–169. IEEE, 2000.
- [8] David E Stewart. Rigid-body dynamics with friction and impact. *SIAM review*, 42(1):3–39, 2000.
- [9] Mihai Anitescu and Florian A Potra. Formulating dynamic multi-rigid-body contact problems with friction as solvable linear complementarity problems. *Nonlinear Dynamics*, 14:231–247, 1997.
- [10] Alp Aydinoglu, Adam Wei, Wei-Cheng Huang, and Michael Posa. Consensus complementarity control for multi-contact mpc, 2024.
- [11] Tobia Marcucci and Russ Tedrake. Warm start of mixed-integer programs for model predictive control of hybrid systems. *IEEE Transactions on Automatic Control*, 66(6):2433–2448, 2020.
- [12] Boyang Deng, Kyle Genova, Soroosh Yazdani, Sofien Bouaziz, Geoffrey Hinton, and Andrea Tagliasacchi. Cvxnet: Learnable convex decomposition. In *Computer Vision Pattern Recognition (CVPR)*, 2020.
- [13] Tao Pang and Russ Tedrake. A robust time-stepping scheme for quasistatic rigid multibody systems. In *2018 IEEE/RSJ International Conference on Intelligent Robots and Systems (IROS)*, pages 5640–5647. IEEE, 2018.
- [14] Mihai Anitescu. Optimization-based simulation of nonsmooth rigid multibody dynamics. *Mathematical Programming*, 105:113–143, 2006.
- [15] Tao Pang and Russ Tedrake. A convex quasistatic time-stepping scheme for rigid multibody systems with contact and friction. In *2021 IEEE International Conference on Robotics and Automation (ICRA)*, pages 6614–6620. IEEE, 2021.
- [16] Adam Paszke, Sam Gross, Soumith Chintala, Gregory Chanan, Edward Yang, Zachary DeVito, Zeming Lin, Alban Desmaison, Luca Antiga, and Adam Lerer. Automatic differentiation in pytorch. In *NIPS-W*, 2017.
- [17] Joel A E Andersson, Joris Gillis, Greg Horn, James B Rawlings, and Moritz Diehl. CasADi – A software framework for nonlinear optimization and optimal control. *Mathematical Programming Computation*, 11(1):1–36, 2019.
- [18] Bernardo Aceituno-Cabezas and Alberto Rodriguez. A global quasi-dynamic model for contact-trajectory optimization in manipulation. 2020.
- [19] Wanxin Jin and Michael Posa. Task-driven hybrid model reduction for dexterous manipulation. *IEEE Transactions on Robotics*, 40:1774–1794, 2024.
- [20] Haozhi Qi, Ashish Kumar, Roberto Calandra, Yi Ma, and Jitendra Malik. In-Hand Object Rotation via Rapid Motor Adaptation. In *Conference on Robot Learning (CoRL)*, 2022.
- [21] OpenAI: Marcin Andrychowicz, Bowen Baker, Maciek Chociej, Rafal Jozefowicz, Bob McGrew, Jakub Pachocki, Arthur Petron, Matthias Plappert, Glenn Powell, Alex Ray, et al. Learning dexterous in-hand manipulation. *The International Journal of Robotics Research*, 39(1):3–20, 2020.
- [22] Tao Chen, Megha Tippur, Siyang Wu, Vikash Kumar, Edward Adelson, and Pulkit Agrawal. Visual dexterity: In-hand reorientation of novel and complex object shapes. *Science Robotics*, 8(84):eadc9244, 2023.
- [23] Arthur Allshire, Mayank Mittal, Varun Lodaya, Viktor Makoviychuk, Denys Makoviichuk, Felix Widmaier, Manuel Wüthrich, Stefan Bauer, Ankur Handa, and Animesh Garg. Transferring dexterous manipulation from gpu simulation to a remote real-world trifinger. In *2022 IEEE/RSJ International Conference on Intelligent Robots and Systems (IROS)*, pages 11802–11809. IEEE, 2022.
- [24] Anusha Nagabandi, Kurt Konolige, Sergey Levine, and Vikash Kumar. Deep dynamics models for learning dexterous manipulation. In *Conference on Robot Learning*, pages 1101–1112. PMLR, 2020.
- [25] Brian Curless and Marc Levoy. A volumetric method for building complex models from range images. In *Proceedings of the 23rd annual conference on Computer graphics and interactive techniques*, pages 303–312, 1996.
- [26] Richard A Newcombe, Shahram Izadi, Otmar Hilliges, David Molyneaux, David Kim, Andrew J Davison, Pushmeet Kohi, Jamie Shotton, Steve Hodges, and Andrew Fitzgibbon. Kinectfusion: Real-time dense surface mapping and tracking. In *2011 10th IEEE international symposium on mixed and augmented reality*, pages 127–136. Ieee, 2011.
- [27] Danny Driess, Jung-Su Ha, Marc Toussaint, and Russ Tedrake. Learning models as functionals of signed-distance fields for manipulation planning. *ArXiv*, abs/2110.00792, 2021.
- [28] Thomas Weng, David Held, Franziska Meier, and Mustafa Mukadam. Neural grasp distance fields for robot manipulation. *IEEE International Conference on Robotics and Automation (ICRA)*, 2023.
- [29] Matthew T Mason. *Mechanics of robotic manipulation*. MIT press, 2001.
- [30] Xianyi Cheng, Eric Huang, Yifan Hou, and Matthew T Mason. Contact mode guided motion planning for quasidynamic dexterous manipulation in 3d. In *2022 International Conference on Robotics and Automation (ICRA)*, pages 2730–2736. IEEE, 2022.
- [31] Tao Pang, H. J. Terry Suh, Lujie Yang, and Russ Tedrake. Planning for contact-rich manipulation via local smoothing of quasi-dynamic contact models. *IEEE Transactions on Robotics*, 39(6):4691–4711, 2023.
- [32] Jia Pan, Sachin Chitta, and Dinesh Manocha. Fcl: A general purpose library for collision and proximity queries. In *2012 IEEE International Conference on Robotics and Automation*, pages 3859–3866. IEEE, 2012.
- [33] Elmer G Gilbert, Daniel W Johnson, and S Sathiya Keerthi. A fast procedure for computing the distance between complex objects in three-dimensional space. *IEEE Journal on Robotics and Automation*, 4(2):193–203, 1988.
- [34] Bartolomeo Stellato, Goran Banjac, Paul Goulart, Alberto Bemporad, and Stephen Boyd. Osqp: An operator splitting solver for quadratic programs. *Mathematical Programming Computation*, 12(4):637–672, 2020.
- [35] Antoine Bambade, Sarah El-Kazdadi, Adrien Taylor, and Justin Carpentier. Prox-qp: Yet another quadratic programming solver for robotics and beyond. In *RSS 2022-Robotics: Science and Systems*, 2022.
- [36] Kevin Tracy, Taylor A Howell, and Zachary Manchester. Differentiable collision detection for a set of convex primitives. In *2023 IEEE International Conference on Robotics and Automation (ICRA)*, pages 3663–3670. IEEE, 2023.
- [37] Khaled Mamou and Faouzi Ghorbel. A simple and efficient approach for 3d mesh approximate convex decomposition. In *2009 16th IEEE international conference on image processing (ICIP)*, pages 3501–3504. IEEE, 2009.
- [38] Louis Montaut, Quentin Le Lidec, Antoine Bambade, Vladimir Petrik, Josef Sivic, and Justin Carpentier. Differentiable collision detection: a randomized smoothing approach. In *2023 IEEE International Conference on Robotics and Automation (ICRA)*, pages 3240–3246. IEEE, 2023.
- [39] Charles Ruizhongtai Qi, Hao Su, Matthias Nießner, Angela Dai, Mengyuan Yan, and Leonidas J. Guibas. Volumetric and multi-view cnns for object classification on 3d data. *CoRR*, abs/1604.03265, 2016.
- [40] Bowen Wen, Jonathan Tremblay, Valts Blukis, Stephen Tyree, Thomas Muller, Alex Evans, Dieter Fox, Jan Kautz, and Stan Birchfield. Bundlesdf: Neural 6-dof tracking and 3d reconstruction of unknown objects. *CVPR*, 2023.
- [41] Jeong Joon Park, Peter Florence, Julian Straub, Richard Newcombe, and Steven Lovegrove. DeepSDF: Learning continuous signed distance functions for shape representation. In *Proceedings of the IEEE/CVF*

- conference on computer vision and pattern recognition*, pages 165–174, 2019.
- [42] Thibault Groueix, Matthew Fisher, Vladimir G. Kim, Bryan Russell, and Mathieu Aubry. AtlasNet: A Papier-Mâché Approach to Learning 3D Surface Generation. In *Proceedings IEEE Conf. on Computer Vision and Pattern Recognition (CVPR)*, 2018.
 - [43] Mark W Spong, Seth Hutchinson, and Mathukumalli Vidyasagar. *Robot modeling and control*. John Wiley & Sons, 2020.
 - [44] Emanuel Todorov, Tom Erez, and Yuval Tassa. Mujoco: A physics engine for model-based control. In *2012 IEEE/RSJ International Conference on Intelligent Robots and Systems*, pages 5026–5033. IEEE, 2012.
 - [45] Edwin Olson. AprilTag: A robust and flexible visual fiducial system. In *Proceedings of the IEEE International Conference on Robotics and Automation (ICRA)*, pages 3400–3407. IEEE, May 2011.
 - [46] Bernd Pfrommer and Kostas Daniilidis. Tag slam: Robust SLAM with fiducial markers. *CoRR*, abs/1910.00679, 2019.
 - [47] Stanford Artificial Intelligence Laboratory et al. Robotic operating system.